Applied Physics Letters

Tuning photoacoustics with nanotransducers via thermal boundary resistance and laser pulse duration

Cite as: Appl. Phys. Lett. **121**, 252201 (2022); https://doi.org/10.1063/5.0135147
Submitted: 16 November 2022 • Accepted: 05 December 2022 • Published Online: 21 December 2022

Michele Diego, Marco Gandolfi, Stefano Giordano, et al.

AIP Publishing

Applied Physics Letters ARTICLE scitation.org/journal/apl

Tuning photoacoustics with nanotransducers via thermal boundary resistance and laser pulse duration

Cite as: Appl. Phys. Lett. **121**, 252201 (2022); doi: 10.1063/5.0135147
Submitted: 16 November 2022 · Accepted: 5 December 2022 ·
Published Online: 21 December 2022

Michele Diego,[1,a)] Marco Gandolfi,[2,3,4] Stefano Giordano,[5] Fabien Vialla,[1] Aurélien Crut,[1] Fabrice Vallée,[1] Paolo Maioli,[1] Natalia Del Fatti,[1,6] and Francesco Banfi[1]

AFFILIATIONS

[1]FemtoNanoOptics Group, Université de Lyon, CNRS, Université Claude Bernard Lyon 1, Institut Lumière Matière, F-69622 Villeurbanne, France
[2]CNR-INO, via Branze 45, 25123 Brescia, Italy
[3]Department of Information Engineering, Università di Brescia, via Branze 38, 25123 Brescia, Italy
[4]Interdisciplinary Laboratories for Advanced Materials Physics (I-LAMP) and Dipartimento di Matematica e Fisica, Università Cattolica del Sacro Cuore, via della Garzetta 48, Brescia I-25133, Italy
[5]Université de Lille, CNRS, Centrale Lille, Université Polytechnique Hauts-de-France, UMR 8520–IEMN–Institut d'Électronique de Microélectronique et de Nanotechnologie, F-59000 Lille, France
[6]Institut Universitaire de France (IUF), F-75005 Paris, France

[a)]**Author to whom correspondence should be addressed:** michele.diego@univ-lyon1.fr

ABSTRACT

The photoacoustic effect in liquids, generated by metal nanoparticles excited with short laser pulses, offers high contrast imaging and promising medical treatment techniques. Understanding the role of the thermal boundary resistance (TBR) and the laser pulse duration in the generation mechanism of acoustic waves is essential to implement efficient photoacoustic nanotransducers. This work theoretically investigates, for the paradigmatic case of water-immersed gold nanocylinders, the role of the TBR and laser pulse duration in the competition between the launching mechanisms: the thermophone and the mechanophone. In the thermophone, the nanoparticle acts as a nanoheater and the wave is launched by water thermal expansion. In the mechanophone, the nanoparticle directly acts as a nanopiston. Specifically, for a gold–water interface, the thermophone prevails under ns light pulse irradiation, while the mechanophone dominates shortening the pulse to the 10 ps regime. For a graphene-functionalized gold–water interface, instead, the mechanophone dominates over the entire range of explored laser pulse durations. The results point to high-TBR, liquid-immersed nanoparticles as potentially efficient photoacoustic nanogenerators, with the advantage of keeping the liquid environment temperature unaltered.

Nanoscale photoacoustics generation in liquids, owing to its potential in nanoimaging and therapeutic applications, is a flourishing topic at the cross-road of condensed matter physics, nanomedicine, and materials science.[1–5] In this context, liquid-immersed metal nanoparticles have proven to be efficient photoacoustic generators due to their tunable optical absorption properties,[6–9] high contrast imaging features,[10,11] and biocompatibility.[12,13] Great efforts have been devoted to optimize the parameters allowing a more efficient photoacoustic conversion, such as size, geometry,[9,14–16] and transducer materials.[17] Yet, despite its relevance for applications, the combined effects of the pulse temporal width, τ_L,[18–20] and the thermal boundary resistance[21–23] (TBR) tunabilities remain relatively unexplored and lack a thorough rationalization.

In brief, the photoacoustic effect of an individual liquid-immersed metal nanoparticle consists of three steps: (i) absorption of the laser pulse by the nanoparticle and its temperature rise, (ii) thermal interaction between the nanoparticle and the liquid environment, and (iii) generation of the acoustic wave in liquid. The acoustic wave in liquid is triggered by two launching mechanisms: the mechanophone and the thermophone effects. The former is due to the thermal expansion of the metal nanoparticle; the latter mechanism is due to the liquid environment expansion with the nanoparticle acting as a

nanoheater. The photoacoustic generation in these systems is typically investigated under ns laser pulse irradiation, in which case the mechanophone contribution is, in most instances, disregarded.[18,24–27] Nevertheless, the mechanophone effect cannot be neglected in general, as recently demonstrated for the case of carbon nanotubes immersed in water.[20] Once the size and composition of the nanoparticles and of the surrounding liquid are fixed by the specific application constraints, the relative contributions of the thermophone vs mechanophone effects may be tuned upon varying the TBR at the nanoparticle/liquid interface (interface engineering) and τ_L, their interplay making the focus of the present work.

We theoretically investigate the role of the thermophone and mechanophone effects in acoustic wave generation for the paradigmatic case of a water-immersed gold nanocylinder (GNC) of radius $R_{gnc} = 10$ nm and of high aspect ratio, because of their relevance in bio-medical applications.[28–34] Formally, the GNC is assumed infinitely extended along its axis, the problem thus being radially symmetric with r the radial coordinate. The model, detailed in the supplementary material, comprises three steps: optics, thermics, and mechanics. As for the optics, the system, at equilibrium at $t = 0$ s, is excited with a laser pulse at 530 nm wavelength, i.e., within water transparency window. The light intensity (W/m^2) has a Gaussian intensity profile, $I(t) = 2\sqrt{\frac{\ln(2)}{\pi}}\frac{\Phi}{\tau_L}\exp\left[-4\ln(2)\frac{(t-t_0)^2}{\tau_L^2}\right]$, where $\Phi = 10$ J/m^2 is the pulse fluence, which is kept constant for all τ_L values, with $\tau_L = 1$ ns, 100 ps, 10 ps its temporal full-width-half-maximum, while the pulse temporal peak occurs at $t_0 = 3\tau_L$. We then calculate the absorbed power density, via the GNC absorption cross section, that serves as the source term for the thermics. The temperature $T(r, t)$ throughout the system (both GNC and water) is then obtained solving the thermal diffusion equation while imposing the continuity of the heat flux at the GNC/water interface, $\vec{q} = \frac{1}{\mathscr{R}}[T(R_{gnc}-, t) - T(R_{gnc}+, t)]\hat{r}$, which is controlled by the TBR, $\mathscr{R}$, with $T(R_{gnc}\pm, t)$ the temperature at the inner $(-)$ and outer $(+)$ side of the interface and $\hat{r}$ its normal vector. $T(r, t)$ serves as the source terms for the mechanics via the thermal expansion coefficients of both the GNC and water, ultimately yielding the pressure, $p(r, t)$, and the radial velocity field, $v_r(r, t)$ in water. With p and v_r at hand, the acoustic Poynting vector, $\mathbf{P}$ (W/m^2), and from it the mechanical energy radiated in water, U, are retrieved. The thermophone and mechanophone contributions to the total $p(r, t)$ and U are calculated forcing to zero the GNC and water thermal expansion coefficients, respectively.

The first conclusion that can be drawn from simulation results is that the mechanophone effect needs to be accounted for. Figure 1 shows $p(t)$ in water, 5 nm from the GNC/water interface, together with the thermophone and mechanophone contributions. The results are for the case of $\tau_L = 1$ ns and $\mathscr{R} = 1 \times 10^{-7}$ m^{2}K/W. The latter is representative of the general cases that might be encountered: its order of magnitude falls between that of the Au/water, 1×10^{-8} m^{2}K/W,[18,35–37] and that of the graphene-functionalized Au/water interface, which has been predicted to be ~ 2 orders of magnitude smaller,[38] we therefore take 1×10^{-6} m^{2}K/W. The thermophone and the mechanophone contributions have similar amplitudes, thus both contributing to the total pressure signal.

We now address the role played by the TBR and τ_L in the relative contribution between these two launching mechanisms. On the thermal side, upon absorption of the laser pulse, the GNC raises its temperature on a timescale τ_L. It cools down on a timescale τ_{th} transferring heat to the proximal water and raising the temperature of the latter. Finally, the GNC and the proximal water diffuse heat to distant water, relaxing to the initial temperature. The timescale τ_{th} has contributions from the TBR and heat diffusion effects arising from the GNC and proximal water thermal impedances.[39] We now discuss what might be intuitively foreseen in the two extreme-case scenarios.

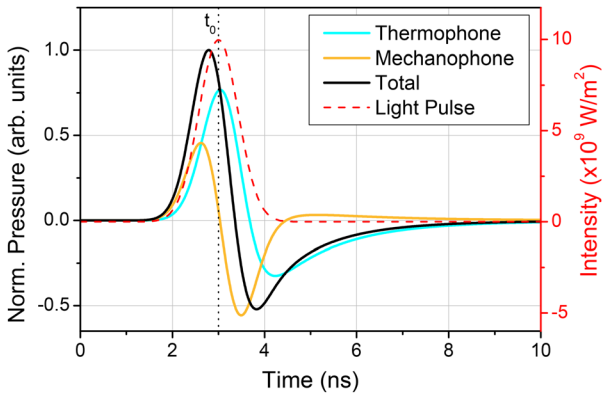

FIG. 1. Left axis: pressure time evolution in water at $r = R_{gnc} + 5$ nm for $\tau_L = 1$ ns, $\mathscr{R} = 1 \times 10^{-7}$ m^{2}K/W. The curves are normalized to the total pressure maximum. Right axis: $I(t)$ (red dashed curve).

For $\tau_{th} \gg \tau_L$, energy from the laser pulse is delivered to the GNC on a timescale τ_L, and, only after a time $\sim\tau_{th}$, the GNC temperature decreases substantially, while delivering heat to the proximal water. That is, on a timescale τ_{th} we should expect a high-temperature GNC, thermally isolated from the surrounding water still at its ambient temperature. On the mechanics side, the thermal expansion of the GNC should be at its maximum. On the contrary, the contribution of water thermal expansion should be at a minimum and set in on a timescale exceeding τ_{th}. The relevance of the mechanophone effect with respect to the thermophone should thus be highest for cases in which $\tau_{th} \gg \tau_L$.

For $\tau_{th} \ll \tau_L$, the situation is the opposite. The laser feeds energy to the GNC on a timescale τ_L, whereas the GNC delivers energy to the proximal water on a much faster timescale, τ_{th}: the GNC absorbs energy from the laser pulse and concomitantly delivers it to the proximal water. In this scenario, the peak GNC temperature should be at its minimum, whereas the proximal water temperature should reach its greatest value. Accordingly, on the mechanics side, the peak thermal expansion of the GNC should be at its minimum and that of proximal water at its maximum. The relevance of the mechanophone effect with respect to the thermophone should thus be lowest for $\tau_{th} \ll \tau_L$.

In first instance, the ratio τ_{th}/τ_L therefore appears as a meaningful metric to inspect the thermophone to mechanophone transition. The TBR is though the *only* material parameter that can be tuned,[40–56] the thermal properties of the GNC and water being fixed. Under a practical stand-point, it is therefore desirable to parameterize the problem in terms of a thermal decay time linked to the TBR only, rather than to τ_{th}, which comprises also the effect of proximal water and GNC thermal impedances. To this end, we link the TBR to the thermal decay time through the expression $\tau_{TBR} = \mathscr{R}R_{gnc}c_p\rho/2$, with c_p and ρ the Au specific heat and mass density, respectively. This relation is

somewhat approximate;[57] nevertheless, it has the merit of providing a rule-of-thumb estimate. In the following, we therefore parameterize simulations results in terms of τ_{TBR}/τ_L rather than τ_{th}/τ_L. We now inspect what happens varying the TBR for a fixed laser pulse duration.

Nanosecond regime. Figure 2 shows the GNC (a) and the proximal water (b) temperature dynamics. The curves are calculated for a fixed value of $\tau_L = 1$ ns while varying the TBR, from 10^{-5} to 10^{-9} m^2K/W, so as to cover the range of τ_{TBR}/τ_L from 10^{-2} to 10^{2}. For increasing τ_{TBR}/τ_L, the GNC maximum temperature, $max\{T_{gnc}(t)\}$, increases from 305 to 377 K, whereas that of proximal water, $max\{T_w(t)\}$, decreases from 300 to 293 K.

The implications of the thermal problem on the competition between the thermophone and mechanophone contributions are shown in panel (c). The histogram shows the mechanical energy radiated in water by the sole thermophone (azure) and sole mechanophone (mustard) effects as a function of τ_{TBR}/τ_L (bottom axis) and TBR (top axis). Energies are normalized to the maximum mechanical energy observed in water in our simulations (i.e., the thermophone contribution of the $\tau_L = 10$ ps, $\tau_{TBR}/\tau_L = 10^{-11}$ case that will be described later). For increasing values of the TBR, acoustic wave generation in water switches from thermophone-dominated for $\tau_{TBR}/\tau_L \lesssim 1$, to mechanophone-dominated for $\tau_{TBR}/\tau_L \gg 1$, $\tau_{TBR}/\tau_L \approx 1$ being a crossover value between the two regimes.

In real case scenarios, the TBR can be tuned engineering the GNC/water interface, and the acoustic wave launching mechanism accordingly, switching for instance from the thermophone for the bare Au/water interface, to the mechanophone for the graphene-functionalized Au/water interface, which cases are indicated by the two inset sketches.

So far, we spanned τ_{TBR}/τ_L for a fixed value of τ_L while varying the TBR. The question then arises as to whether a similar physics holds true also for shorter laser pulses, thus eventually allowing for an additional knob, τ_L, to select the launching mechanism.

Picosecond regime. Figures 3 and 4 are analogous to Fig. 2 but for the cases of $\tau_L = 100$ and 10 ps, respectively. For sake of comparison, the TBR is now varied from 10^{-6} to 10^{-10} m^2K/W and from 10^{-7} to 10^{-11} m^2K/W for the case $\tau_L = 100$ and 10 ps, respectively. These changes allow covering the same range of τ_{TBR}/τ_L as for the case of the 1 ns laser pulse. On the thermal side, Figs. 3(a) and 3(b) and Figs. 4(a) and 4(b) encompass the general trend observed in Figs. 2(a) and 2(b): for increasing τ_{TBR}/τ_L, $max\{T_{gnc}(t)\}$ increases whereas $max\{T_w(t)\}$ decreases. While reducing τ_L, a relevant parameter for the following discussion is δT_{gnc}, defined as the difference between the GNC peak temperatures between the cases of $\tau_{TBR}/\tau_L = 10^2$ and 10^{-2}. δT_{gnc} ranges from 72 K for $\tau_L = 1$ ns, to 27 K for $\tau_L = 10$ ps, because of the increase in the peak temperature for the case of $\tau_{TBR}/\tau_L = 10^{-2}$ while transitioning from Fig. 2(a), across Fig. 3(a) to Fig. 4(a). Among the physical reasons behind this trend is that reducing τ_L for a fixed value of $\tau_{TBR}/\tau_L = 10^{-2}$ implies reducing the TBR, eventually to a point where the interfacial heat transfer is no more the limiting process, the GNC and the proximal water thermal impedances remaining as the only factors controlling the thermal dynamics.[58]

The implications of the thermal problem on the competition between the thermophone and mechanophone contributions are shown in panel (c) of Figs. 3 and 4, for $\tau_L = 100$ and 10 ps, respectively. The striking difference, comparing Figs. 2(c), 3(c), and 4(c), is that the mechanophone contribution dependence on τ_{th}/τ_L weakens substantially upon reducing the pulse temporal width; not

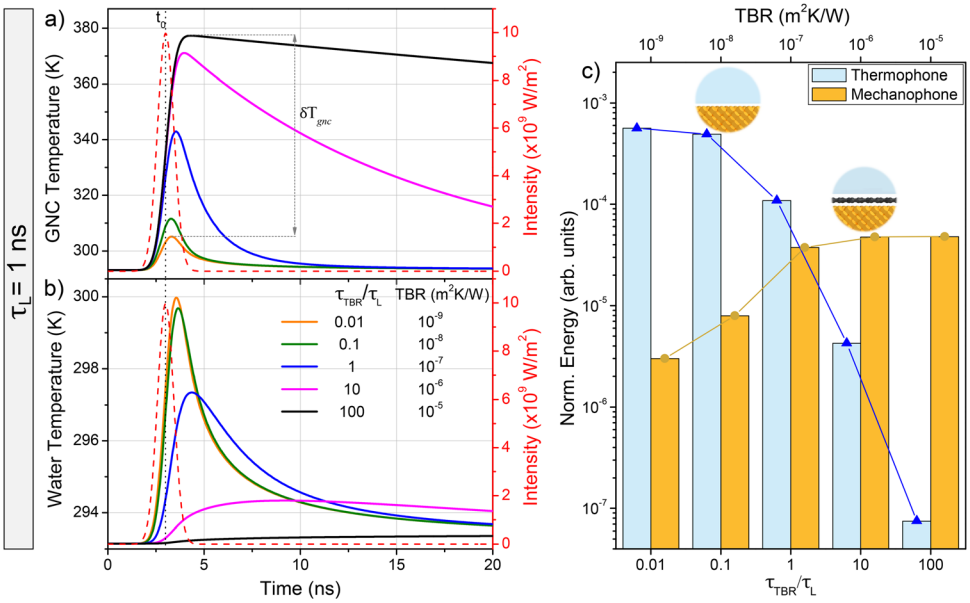

FIG. 2. Laser pulse: $\tau_L = 1$ ns. Panels (a) and (b): temperature time evolution, for increasing values of τ_{TBR}/τ_L and the corresponding TBR values, in the GNC ($r = 0$ nm): panel (a); in proximal water ($r = R_{gnc} + 5$ nm): panel (b). Right axis: $I(t)$ (red dashed line) maximum at the time t_0. δT_{gnc}: difference between the GNC peak temperatures between the cases of $\tau_{TBR}/\tau_L \sim 100$ and 0.01. Panel (c): normalized mechanical energy generated in water by the thermophone and the mechanophone effects for different τ_{TBR}/τ_L (bottom axis) and the corresponding TBRs (top axis). The ratios τ_{TBR}/τ_L are rounded to the first significant figure. Values for Au/water and graphene-functionalized Au/water interface are identified by the two round sketches.

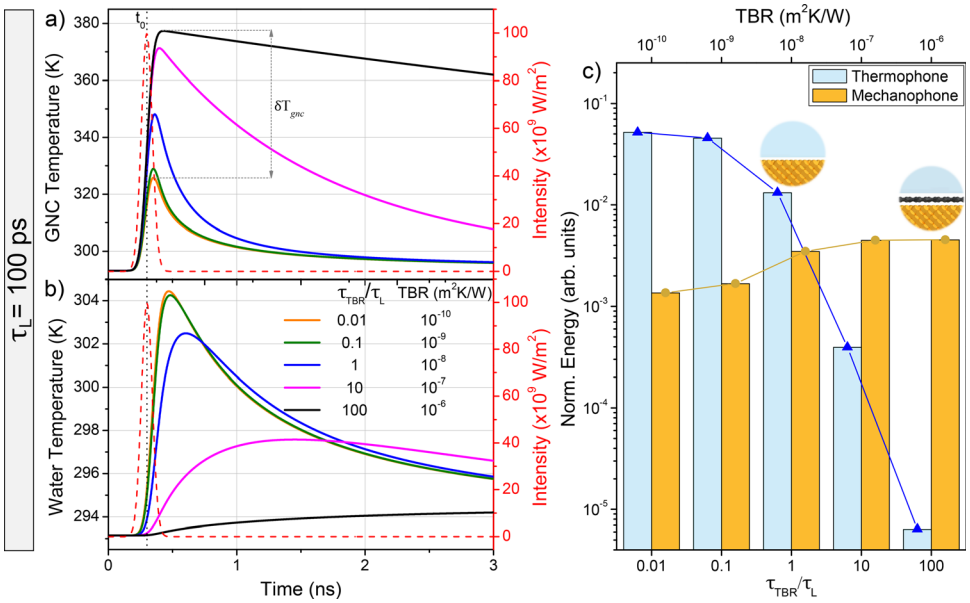

FIG. 3. Laser pulse: $\tau_L = 100$ ps. Same caption as for Fig. 2. The TBR values are varied so as to span the same values of τ_{TBR}/τ_L as for the 1 ns pulse case.

so for the thermophone contribution. Indeed, for the $\tau_L = 1$ ns case, the mechanophone contribution changes by more than an order of magnitude when increasing τ_{TBR}/τ_L from 10^{-2} to 10^2, whereas it changes by a factor of ~2 for the $\tau_L = 10$ ps case. The physical reason stands in the thermal problem. The mechanophone effect is triggered by the GNC thermal expansion. The shorter the laser pulse, the smaller is δT_{gnc}, implying that the peak GNC temperature becomes rather insensitive to the ratio τ_{TBR}/τ_L, and the GNC thermal expansion accordingly.

When exciting with a 100 ps laser pulse, the mechanophone contribution to the radiated acoustic energy in water raises to 23% for the Au GNC/water interface and dominates the graphene-functionalized GNC/water interface, see Fig. 3(c). Further reducing the pulse duration to 10 ps, the mechanophone effect becomes the

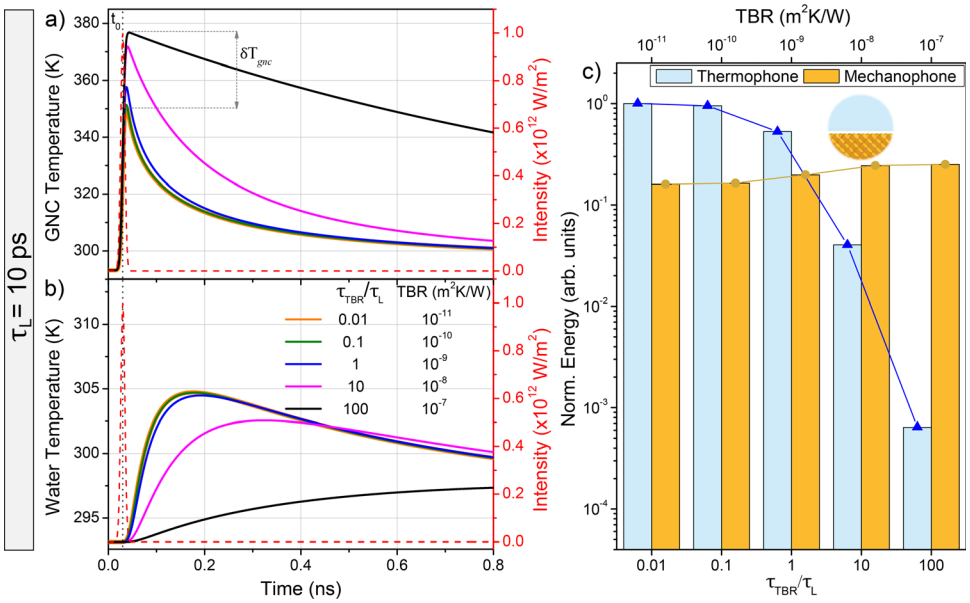

FIG. 4. Laser pulse: $\tau_L = 10$ ps. Same caption as for Fig. 2. The TBR values are varied so as to span the same values of τ_{TBR}/τ_L as for the 1 ns pulse case. In panel (c) the case of the graphene-functionalized Au/water interface is here dominated by the mechanophone effect and is hence not reported.

prevailing mechanism also for the Au GNC/water interface, see Fig. 4(c).[59]

In conclusion, we showed, for the case of a water-immersed Au nanocylinder, that the TBR and the laser pulse duration are two valuable control knobs, allowing us to switch the acoustic wave launching mechanism in water from the thermophone to the mechanophone. The Au/water and graphene-functionalized Au/water interfaces were discussed as realistic show-case scenarios. Importantly, when the mechanophone is the dominant launching effect, the surrounding water temperature increase is minimized. These findings, thus, bear particular importance in situations requiring high frequency acoustic wave generation in water (i.e., short τ_L) while avoiding heating effects of the latter, as is the case for *in vivo* bioimaging and theranostics applications at the nanoscale. It is noteworthy that these findings may be expanded to include other nanosystems.[60,61]

See the supplementary material for the details on the simulations design.

This work was partially supported by the LABEX iMUST (No. ANR-10-LABX-0064) of Université de Lyon within the program "Investissements d'Avenir" (No. ANR-11-IDEX-0007) and by ANR through projects 2D-PRESTO (No. ANR-19-CE09-0027) and ULTRASINGLE (No. ANR-20-CE30-0016).

F.B. acknowledges financial support from CNRS through Délégation CNRS 2021–2022.

AUTHOR DECLARATIONS

Conflict of Interest

The authors have no conflicts to disclose.

Author Contributions

Michele Diego: Conceptualization (lead); Data curation (lead); Formal analysis (lead); Investigation (equal); Methodology (equal); Validation (equal); Writing – original draft (equal). **Marco Gandolfi:** Conceptualization (equal); Formal analysis (equal); Methodology (equal); Validation (equal); Writing – review & editing (equal). **Stefano Giordano:** Conceptualization (equal); Investigation (equal); Validation (equal); Writing – review & editing (equal). **Fabien Vialla:** Conceptualization (equal); Data curation (equal); Funding acquisition (equal); Validation (equal); Visualization (equal); Writing – review & editing (equal). **Aurelien Crut:** Conceptualization (equal); Funding acquisition (equal); Validation (equal); Writing – review & editing (equal). **Fabrice Vallée:** Conceptualization (equal); Funding acquisition (equal); Resources (equal); Validation (equal); Writing – review & editing (equal). **Paolo Maioli:** Conceptualization (equal); Validation (equal); Writing – review & editing (equal). **Natalia Del Fatti:** Conceptualization (equal); Funding acquisition (equal); Resources (equal); Supervision (equal); Validation (equal); Writing – review & editing (equal). **Francesco Banfi:** Conceptualization (equal); Data curation (equal); Funding acquisition (equal); Investigation (equal); Methodology (equal); Project administration (equal); Supervision (equal); Validation (equal); Writing – review & editing (equal).

DATA AVAILABILITY

The data that support the findings of this study are available from the corresponding author upon reasonable request.

REFERENCES

[1]S. Y. Emelianov, P.-C. Li, and M. O'Donnell, "Photoacoustics for molecular imaging and therapy," Phys. Today **62**(5), 34 (2009).
[2]C. Li and L. V. Wang, "Photoacoustic tomography and sensing in biomedicine," Phys. Med. Biol. **54**, R59 (2009).
[3]M. Xu and L. V. Wang, "Photoacoustic imaging in biomedicine," Rev. Sci. Instrum. **77**, 041101 (2006).
[4]L. V. Wang, *Photoacoustic Imaging and Spectroscopy* (CRC Press, 2017).
[5]W. Li and X. Chen, "Gold nanoparticles for photoacoustic imaging," Nanomedicine **10**, 299–320 (2015).
[6]X. Yang, E. W. Stein, S. Ashkenazi, and L. V. Wang, "Nanoparticles for photoacoustic imaging," Wiley Interdiscip. Rev.: Nanomed. Nanobiotechnol. **1**, 360–368 (2009).
[7]Y. Mantri and J. V. Jokerst, "Engineering plasmonic nanoparticles for enhanced photoacoustic imaging," ACS Nano **14**, 9408–9422 (2020).
[8]T. El-Brolossy, T. Abdallah, M. B. Mohamed, S. Abdallah, K. Easawi, S. Negm, and H. Talaat, "Shape and size dependence of the surface plasmon resonance of gold nanoparticles studied by photoacoustic technique," Eur. Phys. J.: Spec. Top. **153**, 361–364 (2008).
[9]R. Garcia-Alvarez, L. Chen, A. Nedilko, A. Sánchez-Iglesias, A. Rix, W. Lederle, V. Pathak, T. Lammers, G. Von Plessen, K. Kostarelos, L. M. Liz-Marzán, A. J. Kuehne, and D. N. Chigrin, "Optimizing the geometry of photoacoustically active gold nanoparticles for biomedical imaging," ACS Photonics **7**, 646–652 (2020).
[10]G. P. Luke, D. Yeager, and S. Y. Emelianov, "Biomedical applications of photoacoustic imaging with exogenous contrast agents," Ann. Biomed. Eng. **40**, 422–437 (2012).
[11]D. Pan, M. Pramanik, A. Senpan, J. S. Allen, H. Zhang, S. A. Wickline, L. V. Wang, and G. M. Lanza, "Molecular photoacoustic imaging of angiogenesis with integrin-targeted gold nanobeacons," FASEB J. **25**, 875–882 (2011).
[12]R. Shukla, V. Bansal, M. Chaudhary, A. Basu, R. R. Bhonde, and M. Sastry, "Biocompatibility of gold nanoparticles and their endocytotic fate inside the cellular compartment: A microscopic overview," Langmuir **21**, 10644–10654 (2005).
[13]A. M. Craciun, M. Focsan, K. Magyari, A. Vulpoi, and Z. Pap, "Surface plasmon resonance or biocompatibility—Key properties for determining the applicability of noble metal nanoparticles," Materials **10**, 836 (2017).
[14]Verawaty and M. Pramanik, "Simulating photoacoustic waves from individual nanoparticle of various shapes using k-wave," Biomed. Phys. Eng. Express **2**, 035013 (2016).
[15]P. Guiraud, S. Giordano, O. Bou Matar, P. Pernod, and R. Lardat, "Thermoacoustic wave generation in multilayered thermophones with cylindrical and spherical geometries," J. Appl. Phys. **129**, 115103 (2021).
[16]A. Ronchi, A. Sterzi, M. Gandolfi, A. Belarouci, C. Giannetti, N. Del Fatti, F. Banfi, and G. Ferrini, "Discrimination of nano-objects via cluster analysis techniques applied to time-resolved thermo-acoustic microscopy," Ultrasonics **114**, 106403 (2021).
[17]T. Lee, H. W. Baac, Q. Li, and L. J. Guo, "Efficient photoacoustic conversion in optical nanomaterials and composites," Adv. Opt. Mater. **6**, 1800491 (2018).
[18]M. Gandolfi, F. Banfi, and C. Glorieux, "Optical wavelength dependence of photoacoustic signal of gold nanofluid," Photoacoustics **20**, 100199 (2020).
[19]A. Prost, F. Poisson, and E. Bossy, "Photoacoustic generation by a gold nanosphere: From linear to nonlinear thermoelastics in the long-pulse illumination regime," Phys. Rev. B **92**, 115450 (2015).
[20]M. Diego, M. Gandolfi, A. Casto, F. M. Bellussi, F. Vialla, A. Crut, S. Roddaro, M. Fasano, F. Vallée, N. Del Fatti, P. Maioli, and F. Banfi, "Ultrafast nano generation of acoustic waves in water via a single carbon nanotube," Photoacoustics **28**, 100407 (2022).
[21]Y.-S. Chen, W. Frey, S. Kim, P. Kruizinga, K. Homan, and S. Emelianov, "Silica-coated gold nanorods as photoacoustic signal nanoamplifiers," Nano Lett. **11**, 348–354 (2011).

[22]T. Repenko, A. Rix, A. Nedilko, J. Rose, A. Hermann, R. Vinokur, S. Moli, R. Cao-Milàn, M. Mayer, G. von Plessen, A. Fery, L. De Laporte, W. Lederle, D. N. Chigrin, and A. J. C. Kuehne, "Strong photoacoustic signal enhancement by coating gold nanoparticles with melanin for biomedical imaging," Adv. Funct. Mater. **28**, 1705607 (2018).
[23]L. Cavigli, A. Milanesi, B. N. Khlebtsov, S. Centi, F. Ratto, N. G. Khlebtsov, and R. Pini, "Impact of Kapitza resistance on the stability and efficiency of photoacoustic conversion from gold nanorods," J. Colloid Interface Sci. **578**, 358–365 (2020).
[24]Y.-S. Chen, W. Frey, S. Aglyamov, and S. Emelianov, "Environment-dependent generation of photoacoustic waves from plasmonic nanoparticles," Small **8**, 47–52 (2012).
[25]K. Shahbazi, W. Frey, Y.-S. Chen, S. Aglyamov, and S. Emelianov, "Photoacoustics of core–shell nanospheres using comprehensive modeling and analytical solution approach," Commun. Phys. **2**, 119 (2019).
[26]P. Guiraud, S. Giordano, O. Bou-Matar, P. Pernod, and R. Lardat, "Multilayer modeling of thermoacoustic sound generation for thermophone analysis and design," J. Sound Vib. **455**, 275–298 (2019).
[27]P. Guiraud, S. Giordano, O. Bou Matar, P. Pernod, and R. Lardat, "Two temperature model for thermoacoustic sound generation in thick porous thermophones," J. Appl. Phys. **126**, 165111 (2019).
[28]W. He, X. Wang, X. Gao, Z. Lu, and J. Song, "Application of gold nanoparticles in photoacoustic imaging," IOP Conf. Ser.: Mater. Sci. Eng. **729**, 012086 (2020).
[29]S. Manohar, C. Ungureanu, and T. G. Van Leeuwen, "Gold nanorods as molecular contrast agents in photoacoustic imaging: The promises and the caveats," Contrast Media Mol. Imaging **6**, 389–400 (2011).
[30]L. Cavigli, M. de Angelis, F. Ratto, P. Matteini, F. Rossi, S. Centi, F. Fusi, and R. Pini, "Size affects the stability of the photoacoustic conversion of gold nanorods," J. Phys. Chem. C **118**, 16140–16146 (2014).
[31]L. Cavigli, A. Cini, S. Centi, C. Borri, S. Lai, F. Ratto, M. de Angelis, and R. Pini, "Photostability of gold nanorods upon endosomal confinement in cultured cells," J. Phys. Chem. C **121**, 6393–6400 (2017).
[32]Y.-S. Chen, Y. Zhao, S. J. Yoon, S. S. Gambhir, and S. Emelianov, "Miniature gold nanorods for photoacoustic molecular imaging in the second near-infrared optical window," Nat. Nanotechnol. **14**, 465–472 (2019).
[33]K. S. Dhada, D. S. Hernandez, W. Huang, and L. J. Suggs, "Gold nanorods as photoacoustic nanoprobes to detect proinflammatory macrophages and inflammation," ACS Appl. Nano Mater. **3**, 7774–7780 (2020).
[34]O. B. Knights, S. Ye, N. Ingram, S. Freear, and J. R. McLaughlan, "Optimising gold nanorods for photoacoustic imaging *in vitro*," Nanoscale Adv. **1**, 1472–1481 (2019).
[35]A. Plech, V. Kotaidis, S. Grésillon, C. Dahmen, and G. Von Plessen, "Laser-induced heating and melting of gold nanoparticles studied by time-resolved x-ray scattering," Phys. Rev. B **70**, 195423 (2004).
[36]T. Stoll, P. Maioli, A. Crut, S. Rodal-Cedeira, I. Pastoriza-Santos, F. Vallée, and N. Del Fatti, "Time-resolved investigations of the cooling dynamics of metal nanoparticles: Impact of environment," J. Phys. Chem. C **119**, 12757–12764 (2015).
[37]B. A. Wilson, S. O. Nielsen, J. H. Randrianalisoa, and Z. Qin, "Curvature and temperature-dependent thermal interface conductance between nanoscale gold and water," J. Chem. Phys. **157**, 054703 (2022).
[38]C. Herrero, L. Joly, and S. Merabia, "Ultra-high liquid–solid thermal resistance using nanostructured gold surfaces coated with graphene," Appl. Phys. Lett. **120**, 171601 (2022).
[39]Due to the intricate relaxation dynamics, τ_{th} escapes a formal definition. A commonly adopted operative approach is to define it as the time necessary for the GNC temperature increase, triggered by a δ-like excitation source, to fall to 1/e of its maximum.[20]
[40]H. Han, S. Mérabia, and F. Müller-Plathe, "Thermal transport at solid–liquid interfaces: High pressure facilitates heat flow through nonlocal liquid structuring," J. Phys. Chem. Lett. **8**, 1946–1951 (2017).
[41]A. Pham, M. Barisik, and B. Kim, "Pressure dependence of Kapitza resistance at gold/water and silicon/water interfaces," J. Chem. Phys. **139**, 244702 (2013).
[42]M. Barisik and A. Beskok, "Temperature dependence of thermal resistance at the water/silicon interface," Int. J. Therm. Sci. **77**, 47–54 (2014).
[43]J. Vera and Y. Bayazitoglu, "Temperature and heat flux dependence of thermal resistance of water/metal nanoparticle interfaces at sub-boiling temperatures," Int. J. Heat Mass Transfer **86**, 433–442 (2015).
[44]F. Banfi, V. Juvé, D. Nardi, S. Dal Conte, C. Giannetti, G. Ferrini, N. D. Fatti, and F. Vallée, "Temperature dependence of the thermal boundary resistivity of glass-embedded metal nanoparticles," Appl. Phys. Lett. **100**, 011902 (2012).
[45]X. Wu, Y. Ni, J. Zhu, N. D. Burrows, C. J. Murphy, T. Dumitrica, and X. Wang, "Thermal transport across surfactant layers on gold nanorods in aqueous solution," ACS Appl. Mater. Interfaces **8**, 10581–10589 (2016).
[46]M. E. Caplan, A. Giri, and P. E. Hopkins, "Analytical model for the effects of wetting on thermal boundary conductance across solid/classical liquid interfaces," J. Chem. Phys. **140**, 154701 (2014).
[47]B. Ramos-Alvarado, S. Kumar, and G. Peterson, "Solid–liquid thermal transport and its relationship with wettability and the interfacial liquid structure," J. Phys. Chem. Lett. **7**, 3497–3501 (2016).
[48]B. H. Kim, A. Beskok, and T. Cagin, "Molecular dynamics simulations of thermal resistance at the liquid-solid interface," J. Chem. Phys. **129**, 174701 (2008).
[49]T. Q. Vo, B. Park, C. Park, and B. Kim, "Nano-scale liquid film sheared between strong wetting surfaces: Effects of interface region on the flow," J. Mech. Sci. Technol. **29**, 1681–1688 (2015).
[50]J.-L. Barrat and F. Chiaruttini, "Kapitza resistance at the liquid–solid interface," Mol. Phys. **101**, 1605–1610 (2003).
[51]H. Hu and Y. Sun, "Effect of nanopatterns on Kapitza resistance at a water-gold interface during boiling: A molecular dynamics study," J. Appl. Phys. **112**, 053508 (2012).
[52]Y. Wang and P. Keblinski, "Role of wetting and nanoscale roughness on thermal conductance at liquid-solid interface," Appl. Phys. Lett. **99**, 073112 (2011).
[53]M. R. Hasan, T. Q. Vo, and B. Kim, "Manipulating thermal resistance at the solid–fluid interface through monolayer deposition," RSC Adv. **9**, 4948–4956 (2019).
[54]O. Yenigun and M. Barisik, "Effect of nano-film thickness on thermal resistance at water/silicon interface," Int. J. Heat Mass Transfer **134**, 634–640 (2019).
[55]B.-Y. Cao, J.-H. Zou, G.-J. Hu, and G.-X. Cao, "Enhanced thermal transport across multilayer graphene and water by interlayer functionalization," Appl. Phys. Lett. **112**, 041603 (2018).
[56]Z. Tian, A. Marconnet, and G. Chen, "Enhancing solid-liquid interface thermal transport using self-assembled monolayers," Appl. Phys. Lett. **106**, 211602 (2015).
[57]Formally, the GNC cooling is mono-exponential with a decay given by this formula, only for a Biot number Bi $\ll 1$ and for isothermal water,[62] i.e. the cooling is limited by the interfacial heat transfer only.
[58]As an extreme case scenario, if we were to nullify the TBR we would have $\tau_{TBR} = 0$. In such a situation, the GNC thermal dynamics is entirely ruled by the GNC and proximal water thermal inertia.
[59]Note however that, even for the 10 ps light pulse case, the mechanophone effect for $\tau_{TBR}/\tau_L = 10^2$ is lower than the thermophone effect for $\tau_{TBR}/\tau_L = 10^{-2}$. At room temperature, water thermal expansion coefficient is ∼five times higher than the gold's one. Water's expansion is then more efficient than gold's, leading to the maximum of the thermophone effect to exceed that of the mechanophone one. We tested that, using the same thermal expansion coefficients for both the GNC and water results in a maximum of the mechanophone effect (occurring at $\tau_{TBR}/\tau_L = 10^2$) to be slightly higher than the maximum thermophone effect (occurring at $\tau_{Th}/\tau_L = 10^{-2}$).
[60]M. Bertolotti and R. Li Voti, "A note on the history of photoacoustic, thermal lensing, and photothermal deflection techniques," J. Appl. Phys. **128**, 230901 (2020).
[61]M. Gandolfi, S. Peli, M. Diego, S. Danesi, C. Giannetti, I. Alessandri, V. Zannier, V. Demontis, M. Rocci, F. Beltram, L. Sorba, S. Roddaro, F. Rossella, and F. Banfi, "Ultrafast photoacoustic nanometrology of InAs nanowires mechanical properties," J. Phys. Chem. C **126**, 6361–6372 (2022).
[62]F. Banfi, F. Pressacco, B. Revaz, C. Giannetti, D. Nardi, G. Ferrini, and F. Parmigiani, "Ab initio thermodynamics calculation of all-optical time-resolved calorimetry of nanosize systems: Evidence of nanosecond decoupling of electron and phonon temperatures," Phys. Rev. B **81**(15), 115426 (2010).